

PAPER

Single UAV-Based Wave Source Localization in NLOS Environments

Shinichi MURATA^{†a)}, *Member* and Takahiro MATSUDA^{†b)}, *Senior Member*

SUMMARY To localize an unknown wave source in non-line-of-sight environments, a wave source localization scheme using multiple unmanned-aerial-vehicles (UAVs) is proposed. In this scheme, each UAV estimates the direction-of-arrivals (DoAs) of received signals and the wave source is localized from the estimated DoAs by means of maximum likelihood estimation. In this study, by extending the concept of this scheme, we propose a novel wave source localization scheme using a single UAV. In the proposed scheme, the UAV moves on the path comprising multiple measurement points and the wave source is sequentially localized from DoA distributions estimated at these measurement points. At each measurement point, with a *moving path planning algorithm*, the UAV determines the next measurement point from the estimated DoA distributions and measurement points that the UAV has already visited. We consider two moving path planning algorithms, and validate the proposed scheme through simulation experiments.

key words: wave source localization, unmanned aerial vehicle, non-line-of-sight, direction of arrival

1. Introduction

Wave source or emitter localization is a technique for localizing unknown transmitters of radio signals [1]–[7]. Wave source localization enables operators to control interference between wireless communication systems, and can be utilized to design reliable wireless networks in several situations such as (1) spectrum sharing in cognitive radio networks, (2) deployment of local 5G systems, and (3) detection of illegal radios:

- (1) In cognitive radio networks, different wireless communication systems share the frequency spectrum by allowing users in secondary systems to access spectrum holes unoccupied by users in the primary system [8]. Wave source localization can be adopted for highly efficient spectrum sharing in space and time [4].
- (2) In the fifth generation mobile communication (5G) system, closed networks, which are called *local 5G* networks, can be operated for users in specific sites such as companies, schools, and municipalities. Base stations in local 5G networks must be deployed without interfering with other wireless systems including already operated local 5G systems. Wave source localization

can be utilized to manage interference in deploying local 5G base stations. In [9], interference assessment using unmanned-aerial-vehicles (UAVs) in private 5G networks such as the local 5G networks is studied. In addition to improving the utilization of frequency resources, wave source localization techniques contribute to the proper management of frequency resources.

- (3) In Japan, wireless communication systems on licensed band are properly managed by the Ministry-of-Internal-Affairs-and-Communications (MIC). However, a few illegal radio stations emitting radio signals without license exist. These illegal radio stations may trigger interference to licensed radio stations. Wave source localization for detecting illegal stations is a key technology to prevent the illegal radio interference. The radio monitoring system DEURAS [10] is operated by MIC to detect and eliminate these illegal radio stations. In [11], a technique for estimating the source of illegal radio waves has been studied.

We consider wave source localization using a UAV with an antenna array. In [6], [7], a wave source localization scheme based on maximum likelihood estimation in non-line-of-sight (NLOS) environments was proposed. In this scheme, which is referred to as the *MLE* scheme, direction-of-arrivals (DoAs) are estimated with array signal processing [12] at multiple measurement points and a wave source is localized with the estimated DoAs based on a property that a distribution of DoAs at a measurement point is more concentrated in the direction of the wave source as the distance between the wave source and the measurement point increases.

Although MLE can localize a wave source in NLOS environments, it still has two technical limitations. One is the computational complexity for solving the likelihood function, which is formulated as a joint probability of the position of the wave source and concentration parameters of DoA distributions at all measurement points. For N measurement points, the likelihood function is a function with $N + 2$ variables. In [6], [7], the wave source is localized by iterative optimization of the likelihood function. The other is how to determine measurement points. The MLE scheme does not have any strategy to determine measurement points, and measurement points are randomly determined within a monitored area.

In this study, we address these two problem and propose a wave source localization scheme with a single UAV

Manuscript received March 22, 2023.

Manuscript revised June 30, 2023.

Manuscript publicized August 1, 2023.

[†]The authors are with Graduate School of Systems Design, Tokyo Metropolitan University, Hino-shi, 191-0065 Japan.

a) E-mail: murata-shinichi@ed.tmu.ac.jp

b) E-mail: takahiro.m@tmu.ac.jp

DOI: 10.1587/transcom.2023EBP3045

by extending MLE scheme. The proposed scheme adopts a simplified estimator instead of the likelihood function, and estimates the position of the wave source by superimposing DoA distributions, each of which is estimated by a simple calculation at each measurement point. Moreover, each measurement point is sequentially determined from the previous measurement points and a tentatively estimated position of the wave source. To determine the measurement points, we propose two *moving path planning algorithms*.

The remainder of this paper is organized as follows. In Sect. 2, related studies on wave source localization methods are reviewed and the contributions of this study are clarified. Section 3 describes the system model and the MLE scheme. In Sect. 4, the wave source localization method using a single UAV is described. In Sect. 5, the performance of the proposed method is evaluated with simulation experiments. In Sect. 6, we summarize this study.

2. Related Work

Several wave source localization methods have been proposed, which can be classified into three approaches: received signal strength (RSS), time-difference-of-arrival (TDOA), and DoA approaches.

In [3], a wave source localization method using RSS was proposed. In this method, multiple UAVs receive signals from multiple wave sources, where each UAV has a directional antenna, and a monitored rectangle region is divided into sub-rectangles. From the angular field of views of UAVs, the relationship between RSSs and the center positions of the sub-rectangles is formulated by a system of linear equations, and the wave sources are localized with compressed sensing [13], [14].

In [1], [2], a wave source localization method using TDOA was proposed. Let t_i denote the time of arrival (ToA) from the wave source to nodes i , and TDOA $t_{i,j}$ ($i \neq j$) is defined as $t_{i,j} = t_i - t_j$. Moreover, let r_i denote the distance between the wave source and node i . The relationship between $t_{i,j}$, r_i , and r_j is then given by $ct_{i,j} = r_i - r_j$, where c denotes the light speed. Based on this relationship, the wave source is localized from multiple measured TDOAs [1]. Fletcher et al. [2] considered a TDOA-based localization scheme, where a wave source is recursively localized with only two UAVs.

DoA-based wave source localization schemes are proposed in [5]–[7]. Takase et al. [5] propose a wave source localization scheme in LOS environments, where each path between a UAV and the wave source includes a direct path by placing the UAV at a sufficient height. Three UAVs are randomly placed within an area and each UAV estimates the DoA of the direct path by adopting compressed sensing. The wave source is localized as the center of gravity in the triangle formed by the estimated DoAs of the direct paths. The MLE and proposed schemes are DoA-based wave source localization schemes in NLOS environments.

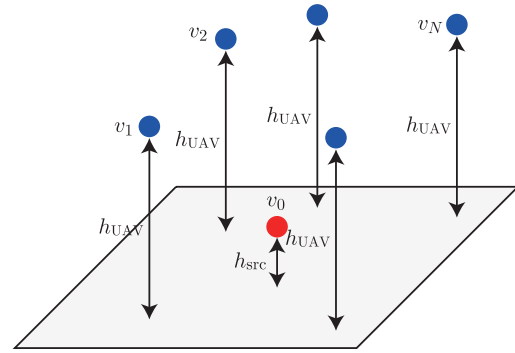


Fig. 1 System model.

3. Wave Source Localization Using Multiple UAVs [6], [7]

3.1 System Model

In this section, we describe the MLE scheme proposed in [6], [7]. Figure 1 illustrates the system model. A single wave source v_0 is located in an area and N UAVs v_n ($n = 1, 2, \dots, N$) are deployed around the area. The wave source is located at the height of h_{src} and all the UAVs are located at the height of h_{UAV} . We assume that $h_{\text{src}} < h_{\text{UAV}}$. Because the wave source and UAVs are placed at different heights, the wave source localization can be considered as a three-dimensional localization problem. However, in this study, we simply consider the two-dimensional problem by projecting locations of the wave source and UAVs onto the two-dimensional space $\mathcal{A} \subset \mathbb{R}^2$. Let $\mathbf{r}_0 = (x, y)^\top \in \mathcal{A}$ denote the location of the wave source v_0 and $\mathbf{r}_n = (x_n, y_n)^\top \in \mathcal{A}$ ($n = 1, 2, \dots, N$) denote the locations of UAVs v_n . Although wave sources may move in actual situations, to investigate the basic performance of the proposed method, we assume the wave source as stationary, that is, the position of the wave source is fixed at \mathbf{r}_0 or the wave source moves at a sufficiently slower speed than the UAV.

A signal transmitted from the wave source v_0 is propagated on a multipath channel. Let Θ_n denote the random variable to represent a DoA at UAV v_n . We assume that Θ_n follows a *von-Mises* distribution, which is known as a unimodal circular distribution [17], and the probability density function $p_{\Theta_n}(\theta)$ of Θ_n is expressed as

$$p_{\Theta_n}(\theta \mid \mu_n, \kappa_n) \triangleq \Pr(\Theta_n = \theta \mid \mu_n, \kappa_n) \\ = \frac{1}{2\pi I_0(\kappa_n)} \exp\{\kappa_n \cos(\theta - \mu_n)\},$$

where μ_n ($0 \leq \mu \leq 2\pi$) and κ_n ($\kappa_n \geq 0$) denote the mean direction and the concentration parameter, respectively, while $I_\nu(\kappa_n)$ represents the ν -th order modified Bessel function of the first kind. As $\kappa_n \rightarrow 0$, $p_{\Theta_n}(\theta)$ converges to the uniform distribution of $\theta \in [0, 2\pi]$, and $\kappa_n \rightarrow \infty$, $p_{\Theta_n}(\theta)$ tends to the point distribution at μ_n .

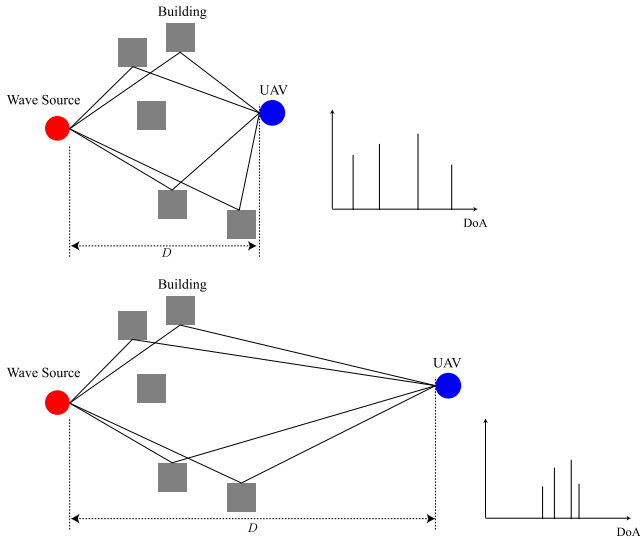


Fig. 2 Relationship between DoA distribution and distance D between UAV and wave source.

In the MLE scheme, DoAs are estimated at each UAV with a compressed sensing-based DoA estimator, which is described in Sect. 3.2, and v_0 is localized from the estimated DoAs. Let $\hat{\theta}_n^{(k)}$ ($n = 1, 2, \dots, N$, $k = 1, 2, \dots, K_n$) denote the k -th estimated DoA at v_n , where K_n represents the number of estimated DoAs at v_n . From the set $\{\hat{\theta}_n^{(k)} \mid n = 1, 2, \dots, N, k = 1, 2, \dots, K_n\}$ of the estimated DoAs, r_0 is estimated by minimizing the log-likelihood function, which is described in Sect. 3.3.

3.2 DoA Estimation

DoA estimation techniques have been studied extensively, and several techniques have been proposed [12]. In this study, we adopt a compressed sensing-based DoA estimation technique [19], [20]. Compressed sensing [13], [14] is a technique for solving an under-determined linear inverse problem under the assumption that an unknown vector is sparse. Regarding the DoA estimation using UAVs, compressed sensing is effective because it is difficult for UAVs to implement several antenna elements owing to the limitation of the payload and hardware complexity.

In this study, we consider that each UAV implements a UCA (Uniform Circular Array) as shown in Fig. 3, where there are L antenna elements with the inter-element distance d . Let (α_l, β_l) and ψ_k ($k = 1, 2, \dots, K$) denote the coordinate of the l -th antenna element and incident angles, respectively. We define $\mathbf{a}(\psi_k) = (a_1(\psi_k) a_2(\psi_k) \cdots a_L(\psi_k))^T$ as the steering vector corresponding to the k -th incident angle, where $a_l(\psi_k)$ is defined as

$$a_l(\psi_k) = \exp\left(-j \frac{2\pi}{\lambda} (\alpha_l \cos \psi_k + \beta_l \sin \psi_k)\right),$$

where λ denotes the wavelength of signals. We also define $\mathbf{y} = (y_1 y_2 \cdots y_L)^T$ and $\mathbf{x} = (x_1 x_2 \cdots x_K)^T$, where y_l ($l = 1, 2, \dots, L$) denotes the received signal at the l -th an-

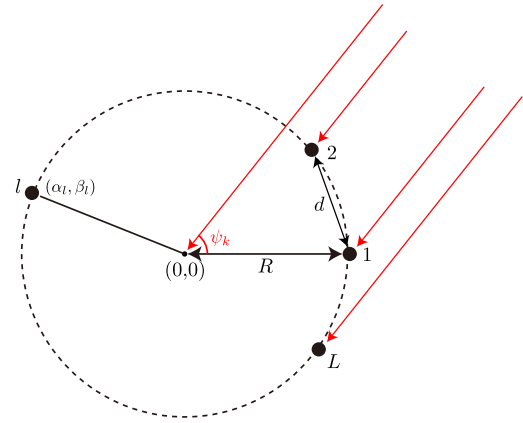


Fig. 3 Geometry of UCA.

tenna element and x_k ($k = 1, 2, \dots, K$) denotes the complex magnitude of the source signal corresponding to the k -th incident angle. The relationship between \mathbf{y} and \mathbf{x} is then expressed as

$$\mathbf{y} = \mathbf{A}\mathbf{x} + \mathbf{w},$$

$$\mathbf{A} = (\mathbf{a}(\psi_1) \mathbf{a}(\psi_2) \cdots \mathbf{a}(\psi_K)),$$

where \mathbf{w} denotes the noise vector.

For given \mathbf{y} and \mathbf{A} , \mathbf{x} can be estimated by solving the following optimization problem:

$$\min_{\mathbf{x}} \frac{1}{2} \|\mathbf{y} - \mathbf{A}\mathbf{x}\|_2^2 + \mu \|\mathbf{x}\|_1, \quad (1)$$

where $\|z\|_p$ ($p = 1, 2$) represents the ℓ_p norm of vector z and μ represents the parameter which control the difference between the squared error and the ℓ_p norm. And $\|z\|_p$ is expressed as

$$\|z\|_p = \left(\sum_{n=1}^N |z_n|^p \right)^{1/p}.$$

To solve Eq.(1), we adopt fast iterative shrinkage thresholding algorithm (FISTA) [21]. By employing FISTA, estimation $\hat{\mathbf{x}} = (\hat{x}_1 \hat{x}_2 \cdots \hat{x}_K)^T$ of \mathbf{x} is obtained as a sparse vector. Let $\{\hat{x}_{i_1} \hat{x}_{i_2} \cdots \hat{x}_{i_{K_n}}\}$ denote the set of the non-zero elements in $\hat{\mathbf{x}}$, where K_n ($K_n \leq K$) represents the number of non-zero elements. The set $\mathcal{T}_n = \{\hat{\theta}_n^{(k)} \mid k = 1, 2, \dots, K_n\}$ of estimated DoAs is expressed as

$$\hat{\theta}_n^{(k)} = \psi_{i_k} \quad (k = 1, 2, \dots, K_n, n = 1, 2, \dots, N).$$

3.3 Maximum Likelihood Estimation for Wave Source Localization

Figure 4 illustrates the relationship between the position \mathbf{r}_n of UAV v_n and position \mathbf{r}_0 of the wave source v_0 . We define \mathbf{e}_n ($\|\mathbf{e}_n\|_2 = 1, n = 1, 2, \dots, N$) as the *reference vector* of v_n . The direction of the wave source v_0 from v_n is given by $\phi_n(\mathbf{r}_0)$, where for $\mathbf{r} \in \mathcal{A}$ ($\mathbf{r} \neq \mathbf{r}_n$), $\phi_n(\mathbf{r})$ is defined as

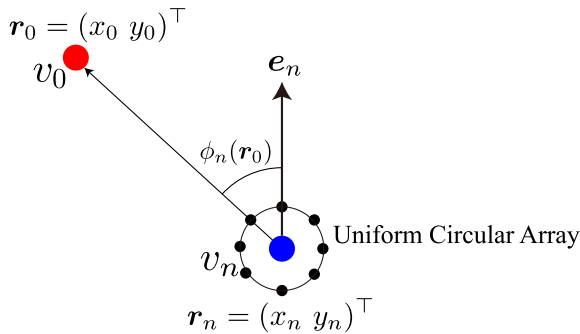


Fig. 4 Relative relationships of positions between a UAV and wave source.

$$\phi_n(\mathbf{r}) = \cos^{-1} \left(\frac{(\mathbf{r} - \mathbf{r}_n)^\top \mathbf{e}_n}{\|\mathbf{r} - \mathbf{r}_n\|_2} \right).$$

In [16], under an assumption that a direct path from a transmitter to a receiver is infinitely attenuated, DoAs are modeled by a Gaussian distribution with the mean oriented to the wave source. By adopting this idea, the ML scheme localizes the wave source by modeling DoAs at each UAV with a von-Mises distribution. We assume that $\hat{\theta}_n^{(k)}$ ($k = 1, 2, \dots, K_n$) follows the von-Mises distribution with mean direction $\phi_n(\mathbf{r}_0)$ and concentration parameter κ_n , and then define the likelihood function $F(\mathbf{r}_0, \boldsymbol{\kappa})$ as

$$F(\mathbf{r}_0, \boldsymbol{\kappa}) = \prod_{n=1}^N \prod_{k=1}^{K_n} p_{\Theta_n}(\hat{\theta}_n^{(k)} | \phi_n(\mathbf{r}_0), \kappa_n),$$

in addition the log-likelihood function $\mathcal{F}(\mathbf{r}_0, \boldsymbol{\kappa})$ is expressed as

$$\begin{aligned} \mathcal{F}(\mathbf{r}_0, \boldsymbol{\kappa}) &= \log \left(\prod_{n=1}^N \prod_{k=1}^{K_n} p_{\Theta_n}(\hat{\theta}_n^{(k)} | \phi_n(\mathbf{r}_0), \kappa_n) \right) \\ &= \sum_{n=1}^N \sum_{k=1}^{K_n} \log \left(p_{\Theta_n}(\hat{\theta}_n^{(k)} | \phi_n(\mathbf{r}_0), \kappa_n) \right) \\ &= \sum_{n=1}^N \sum_{k=1}^{K_n} \left\{ \kappa_n \cos(\hat{\theta}_n^{(k)} - \phi_n(\mathbf{r}_0)) \right. \\ &\quad \left. - \log(I_0(\kappa_n)) - \log(2\pi) \right\}, \end{aligned}$$

where $\boldsymbol{\kappa} = (\kappa_1 \kappa_2 \dots \kappa_N)$. The wave source is localized by determining the optimal \mathbf{r}_0 and $\boldsymbol{\kappa}$ to maximize $\mathcal{F}(\mathbf{r}_0, \boldsymbol{\kappa})$. In [7], an iterative algorithm is adopted to optimize \mathbf{r}_0 and $\boldsymbol{\kappa}$ alternatively.

4. Wave Source Localization Using Single UAV in NLOS Environments

4.1 Overview of the Proposed Scheme

Figure 5 illustrates the basic idea of the proposed wave source localization scheme using single UAV. In the ML scheme described in the previous section, the likelihood function $F(\mathbf{r}_0, \boldsymbol{\kappa})$ comprises multiple probability density functions

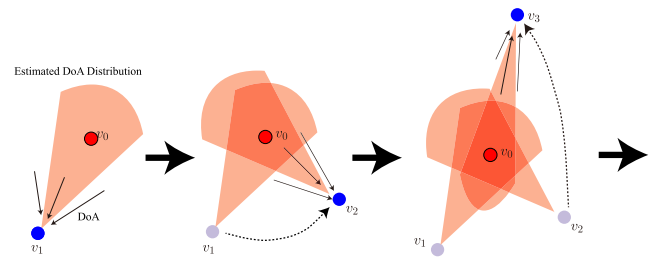


Fig. 5 Wave source localization using single UAV.

$p_{\Theta_n}(\theta | \phi_n(\mathbf{r}_0), \kappa_n)$ ($n = 1, 2, \dots, N$), and from DoAs estimated at multiple UAVs, the wave source is localized by optimizing the log-likelihood function. However, in the proposed scheme, a single UAV moves to multiple measurement points and DoAs are estimated at each measurement point. From the estimated DoAs, the parameters of the von-Mises distribution are estimated independently at each measurement point. Subsequently, the wave source is localized by superimposing the von-Mises distributions.

4.2 Wave Source Localization with Single UAV

We re-define \mathbf{r}_n as the position of the UAV at the n -th measurement point ($n = 1, 2, \dots, N$) and $\mathcal{T}_n = \{\hat{\theta}_n^{(k)} | k = 1, 2, \dots, K_n\}$ as the set of DoAs estimated at \mathbf{r}_n . We assume that DoAs at \mathbf{r}_n follows the von-Mises distribution $p_{\Theta_n}(\theta | \hat{\mu}_n, \hat{\kappa}_n)$, where $\hat{\mu}_n$ and $\hat{\kappa}_n$ represent the mean direction and concentration parameter estimated from \mathcal{T}_n , respectively. Via the maximum likelihood estimation, $\hat{\mu}_n$ and $\hat{\kappa}_n$ are obtained by the following equations [17]

$$\tan \hat{\mu}_n = \frac{\sum_{k=1}^{K_n} \sin \hat{\theta}_n^{(k)}}{\sum_{k=1}^{K_n} \cos \hat{\theta}_n^{(k)}}, \quad (2)$$

$$\begin{aligned} \frac{I_1(\hat{\kappa}_n)}{I_0(\hat{\kappa}_n)} &= \left(\frac{1}{K_n} \sum_{k=1}^{K_n} \cos \hat{\theta}_n^{(k)} \right) \cos \hat{\mu}_n \\ &\quad + \left(\frac{1}{K_n} \sum_{k=1}^{K_n} \sin \hat{\theta}_n^{(k)} \right) \sin \hat{\mu}_n. \end{aligned} \quad (3)$$

For $\mathbf{r} \in \mathcal{A}$, we define $Q(\mathbf{r})$ as

$$\begin{aligned} Q(\mathbf{r}) &= \prod_{n=1}^N q_n(\mathbf{r}), \\ q_n(\mathbf{r}) &= p_{\Theta_n}(\phi_n(\mathbf{r}) | \hat{\mu}_n, \hat{\kappa}_n) \quad n = 1, 2, \dots, N, \end{aligned}$$

where $q_n(\mathbf{r})$ indicates the possibility that the wave source exists. \mathbf{r}_0 is estimated as \mathbf{r} that maximizes $Q(\mathbf{r})$, i.e.,

$$\hat{\mathbf{r}}_0 = \arg \max_{\mathbf{r}} Q(\mathbf{r}).$$

We refer to the above estimator as the *simplified estimator* to distinguish it from the MLE scheme. The simplified estimator and MLE scheme differ from the two perspectives. First, while the MLE scheme estimates \mathbf{r}_0 and $\boldsymbol{\kappa}$ with the

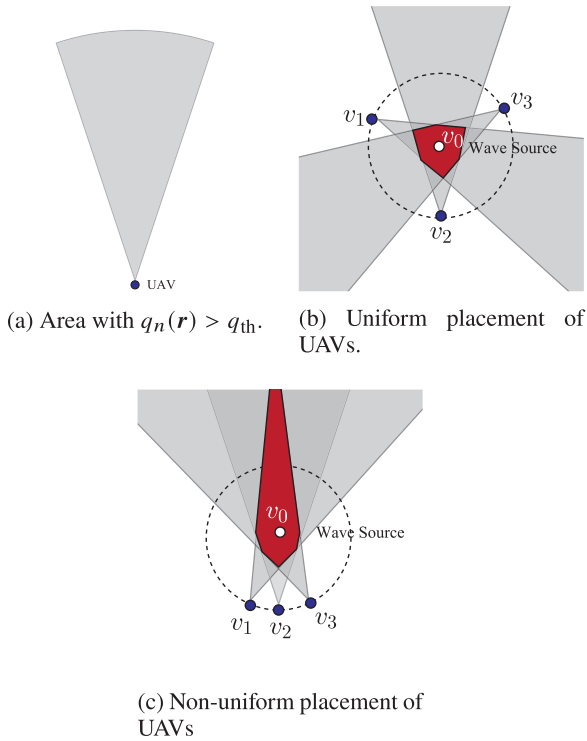


Fig. 6 Influence of measurement points on estimation error.

iterative algorithm, the proposed scheme can estimate these values by simply solving Eqs. (2) and (3). Second, the proposed method can sequentially localize the wave source by determining measurement points from the tentatively estimated position. In this study, we consider two algorithms for determining an efficient moving path of the UAV, as described in the following subsections.

4.3 Efficient Moving Path Configuration for UAV

Owing to the limited battery power of the UAV, a moving path with a shorter distance should be established. Hence, before describing the algorithms to establish the moving path, we discuss how positions of measurement points influence the localization performance in terms of *direction uniformity* and *distance variation*. We define $\mathcal{A}_n(q_{th}) = \{\mathbf{r} \mid q_n(\mathbf{r}) > q_{th}\}$ as a *potential area* that the wave source exists with a higher probability, as illustrated in Fig. 6(a), and $\mathcal{A}(q_{th}) = \bigcap_{n=1}^3 \mathcal{A}_n(q_{th})$, which is the area obtained by superimposing potential areas for three measurement points.

(1) Direction Uniformity

Figures 6(b) and 6(c) present two examples of measurement points placed in a circle. The measurement points are uniformly placed in Fig. 6(b); however, they are placed closely in Fig. 6(c). In these figures, the red areas correspond to $\mathcal{A}(q_{th})$. From these figures, we infer that the non-uniform placement causes a wider area of $\mathcal{A}(q_{th})$.

(2) Distance Variation

Figure 7 presents another example of measurement points,

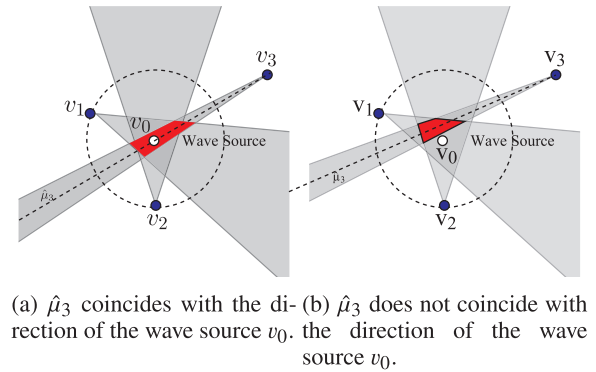


Fig. 7 Influence of distance variation on estimation error.

where one measurement point is placed farther away from the wave source than the other two measurement points. Although $\hat{\mu}_3$ coincides with the direction of the wave source v_0 in Fig. 7(a), $\hat{\mu}_3$ does not in Fig. 7(b). The variance of DoAs can be modeled with a decreasing function of distance between the wave source and the measurement point [7], [16]. Therefore, if several measurement points are placed far from the wave source, these measurement points may significantly influence the performance of the wave source localization. In Fig. 7(b), we observe that the red area does not include the wave source, which implies that the localization error may increase.

From the above discussion, the moving path planning algorithms, which are described in the following two subsections, are based on two ideas:

- measurement points on a moving path surround the tentatively estimated wave source, and
- they are located at comparable distances to the wave source.

In this study, the two moving path planning algorithms are proposed. Algorithm 1 sets the measurement points on a circle centered at a tentatively estimated wave source. Algorithm 2 combines multiple polygons, and the measurement points are placed at the vertices of each polygon.

4.4 Moving Path Planning Algorithm 1

Figure 8 illustrates the moving path planning algorithm 1. Let $\hat{\mathbf{r}}_0^{(n)}$ denote the tentatively estimated position of the wave source obtained after the n -th measurement point. We define ψ_n ($n = 2, 3, \dots$) as the angle between two vectors $\mathbf{r}_n - \hat{\mathbf{r}}_0^{(n)}$ and $\mathbf{r}_{n+1} - \hat{\mathbf{r}}_0^{(n)}$. The $(n + 1)$ -th measurement point \mathbf{r}_{n+1} is determined with $\hat{\mathbf{r}}_0^{(n)}$, \mathbf{r}_{n-1} , and \mathbf{r}_n . Specifically, the algorithm 1 sets \mathbf{r}_{n+1} such that $\|\mathbf{r}_{n+1} - \hat{\mathbf{r}}_0^{(n)}\| = D$ and $\psi_{n+1} + \psi_n = \pi/2$. The algorithm 1 is described as follows:

1. The origin O is set to an arbitrary point in the area.
2. Set $n := 1$. \mathbf{r}_1 is set randomly, and a set $\mathcal{T}_1 = \{\hat{\theta}_1^{(k)} \mid k = 1, 2, \dots, K_1\}$ of DoAs is estimated at \mathbf{r}_1 with the compressed sensing-based DoA estimator described in Sect. 3.2.

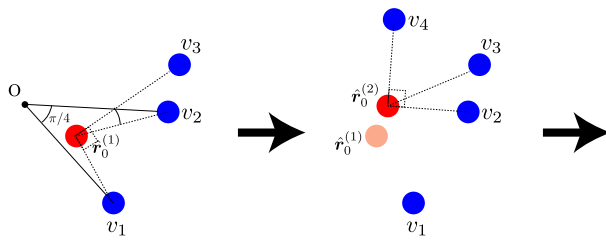


Fig. 8 Moving path planning algorithm 1.

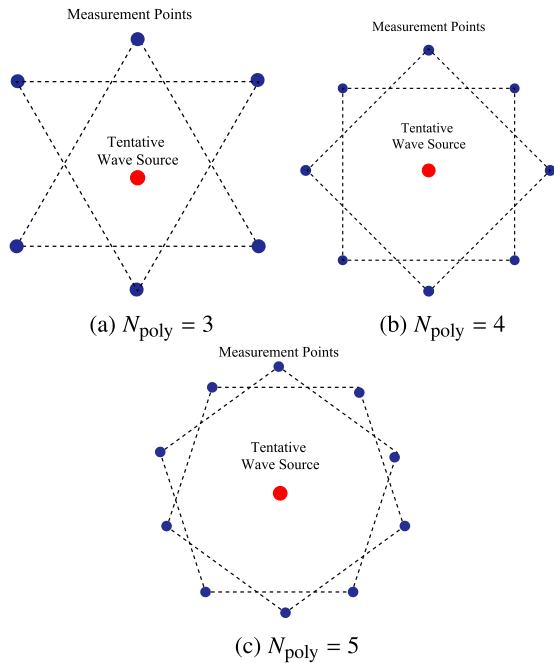


Fig. 9 Idea of moving path planning algorithm 2.

3. Set $n := 2$. \mathbf{r}_2 is set by rotating \mathbf{r}_1 $\pi/4$ around the origin O , and a set $\mathcal{T}_2 = \{\hat{\theta}_2^{(k)} \mid k = 1, 2, \dots, K_2\}$ of DoAs is estimated at \mathbf{r}_2 .
4. A tentative position $\hat{\mathbf{r}}_0^{(2)}$ of the wave source is obtained with estimated DoAs at \mathbf{r}_1 and \mathbf{r}_2 .
5. Set $n := n + 1$. \mathbf{r}_n is set such that $\|\mathbf{r}_n - \hat{\mathbf{r}}_0^{(n-1)}\| = D$ and $\psi_n + \psi_{n-1} = \pi/2$. A set $\mathcal{T}_n = \{\hat{\theta}_n^{(k)} \mid k = 1, 2, \dots, K_n\}$ of DoAs is estimated at \mathbf{r}_n , and $\mathbf{r}_0^{(n)}$ is estimated from $\{\mathcal{T}_{n'} \mid n' = 1, 2, \dots, n\}$ with the estimator described in Sect. 4.2.
6. Terminate the algorithm if $n = N$; otherwise, go to step 5.

4.5 Moving Path Planning Algorithm 2

Figure 9 illustrates the concept of the moving path planning algorithm 2, where measurement points are placed at vertices on multiple polygons. Let N_{poly} denote the number of vertices of each polygon, where Figs. 9(a), 9(b), and 9(c) correspond to $N_{\text{poly}} = 3$ (triangle), $N_{\text{poly}} = 4$ (quadrilateral), and $N_{\text{poly}} = 5$ (pentagon), respectively. We define $L_{n_1, n_2} = \|\mathbf{r}_{n_1} - \mathbf{r}_{n_2}\|$ ($n_1, n_2 = 1, 2, \dots, N$). The algorithm 2

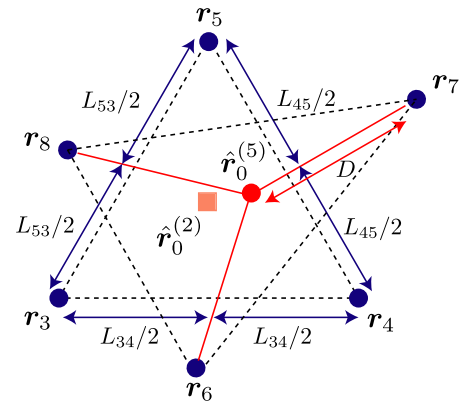


Fig. 10 Moving path planning algorithm 2 for $N_{\text{poly}} = 3$.

is described as follows.

1. By adopting the same procedure as presented in Steps 1–4 of algorithm 1, measurement points, \mathbf{r}_1 and \mathbf{r}_2 , and tentative measurement points $\mathbf{r}_0^{(2)}$ are determined. Set $n := 2$.
2. Set measurement points \mathbf{r}_{n+i} ($i = 1, 2, \dots, N_{\text{poly}}$) as the measurement points corresponding to vertices on a regular polygon with N_{poly} and $\|\mathbf{r}_{n+i} - \mathbf{r}_0^{(n)}\| = D$ for $\forall i = 1, 2, \dots, N_{\text{poly}}$.
3. Estimate \mathcal{T}_{n+i} ($i = 1, 2, \dots, N_{\text{poly}}$) at \mathbf{r}_{n+i} . The tentative position $\mathbf{r}_0^{(n+N_{\text{poly}})}$ of the wave source is estimated from $\{\mathcal{T}_{n'} \mid n' = 1, 2, \dots, N_{\text{poly}} + 2\}$. Set $n := n + N_{\text{poly}}$ and $k := 1$.
4. Set $n_1 = n + k - N_{\text{poly}}$, and $n_2 = n_1 + 1$ if $k < N_{\text{poly}}$, $n_2 = n + 1 - N_{\text{poly}}$ if $k = N_{\text{poly}}$.
5. Set measurement points \mathbf{r}_{n+k} as $\|\mathbf{r}_{n+k} - \hat{\mathbf{r}}_0^{(n)}\| = D$ and $\mathbf{r}_{n+k} - \hat{\mathbf{r}}_0^{(n)}$ crosses the midpoint of \mathbf{r}_{n_1} and \mathbf{r}_{n_2} .
6. If $k < N_{\text{poly}}$, set $k := k + 1$ and go to step 4.
7. Estimate \mathcal{T}_{n+i} ($i = 1, 2, \dots, N_{\text{poly}}$) at \mathbf{r}_{n+i} . The position \mathbf{r}_0 of the wave source is estimated from $\{\mathcal{T}_{n'} \mid n' = 1, 2, \dots, 2N_{\text{poly}} + 2\}$.

Figure 10 presents an example of measurement points obtained by algorithm 2 for $N_{\text{poly}} = 3$. Note that the number N of measurement points is given by $N = 2N_{\text{poly}} + 2$ in algorithm 2, while the arbitrary number of measurement points can be set in algorithm 1.

5. Simulation Experiments

5.1 Simulation Environments

Simulation experiments are conducted to evaluate the performance of the proposed single UAV-based wave source localization scheme. The proposed scheme adopts two different ideas from the MLE scheme. One is that the proposed scheme employs the simplified estimator described in Sect. 4.2. To evaluate the effect of the simplified estimator, we compare the performance of the proposed scheme with that of the MLE scheme by setting the same measurement

Table 1 Wave source localization schemes evaluated with simulation experiments.

	Estimator	Measurement points
SingleUAV1	Simple	Algorithm 1
SingleUAV2	Simple	Algorithm 2
ML1	ML	Same as SingleUAV1
ML2	ML	Same as SingleUAV2
SingleUAVRandom	Simple	Random
MLRandom	ML	Random

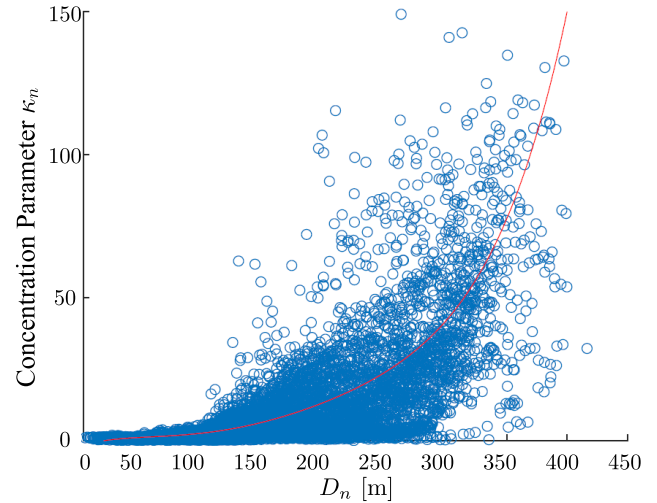
points as the proposed scheme. The other is that measurement points are sequentially placed by adopting the moving path planning algorithm 1 or 2 described in the previous section. To determine the effect of the moving path planning algorithms, we evaluate the performance of the simplified estimator and the MLE scheme for randomly placed measurement points. In Table 1, we summarize the wave source localization schemes evaluated in the simulation experiments. In the table, “Simple” and “ML” represent the simplified estimator explained in Sect. 4.2 and the maximum likelihood estimator explained in Sect. 3, respectively. “Algorithm 1”, “Algorithm 2”, and “Random” represent the moving path planning algorithm 1, 2, and random placement of measurement points, respectively.

We assume that the UAV has a UCA with element spacing $d = 0.5\lambda$, and the number L of antenna elements is set to $L = 10$. The steering vector includes λ of incident signals. This implies that the proposed method requires the center frequency of the signals transmitted from the wave source. Therefore, before applying the proposed method, the center frequency must be obtained. The method to obtain the center frequency depends on situations in which the proposed method is applied. For example, in spectrum sharing within cognitive radio networks, the center frequency is obtained by that of the secondary system. In an illegal radio detection system, by analyzing the frequency spectrum, the center frequency must be identified in advance. In this study, we assume an ideal situation that the correct center frequency is known in advance.

We set $N_{\text{poly}} = 3$ for the moving path planning algorithm 2, i.e., $N = 8$. To evaluate the wave source localization schemes with the same resource, we set $N = 8$ for the moving path planning algorithm 1. We consider two models for DoAs at each reception point: the *probabilistic* and the *ray-tracing*. In the probabilistic model, DoAs at each reception point are generated according to the von-Mises distribution. In the ray-tracing model, DoAs are generated by utilizing a ray-launching-based ray-tracing radio propagation simulator.

(1) Probabilistic Model

The simulation area is set as a $900 \text{ [m]} \times 900 \text{ [m]}$ area, and the wave source is set in the center of the area. DoAs at measurement point v_n ($n = 1, 2, \dots, N$) are generated by the von-Mises distribution with mean value μ_n and concentration parameter κ_n . μ_n is set to coincide with the direction of the wave source. κ_n can be defined as an increasing function of the distance $D_n = \|\mathbf{r}_n - \mathbf{r}_0\|$ between measurement

**Fig. 11** Relationship between distance $D_n = \|\mathbf{r}_n - \mathbf{r}_0\|$ and concentration parameter κ_n [7].**Table 2** Parameter set.

Coefficient	Value
α_3	2.01×10^{-7}
α_2	-0.0001
α_1	0.021
α_0	-0.221

point v_n and wave source v_0 [7], [16]. We determined the shape of function using ray-tracing simulation results. The model used for the simulation corresponds to Furumachi-area in Niigata city. The area is delimited by a 5-m grid, and ray-tracing simulations are performed with each point on the grid as a receiving point. The concentration parameters of the von Mises distribution at the NLOS points are plotted as a scatter plot as shown in Fig. 11. The red curve in the figure represents a regression curve with the cubic polynomial, expressed in equation, where we adopt the same parameter set of the regression curve as in [7]. The parameter sets are shown in Table 2.

$$\kappa_n(D_n) = \alpha_3 D_n^3 + \alpha_2 D_n^2 + \alpha_1 D_n + \alpha_0. \quad (4)$$

In the probabilistic model, the DoAs at each receiving point are provided according to the von Mises distribution. The mean value μ_n corresponds to the direction of the wave source and concentration parameter κ_n of the distribution is obtained from Eq. (4). The number of directions of arrival at each receiving point is set to 10, and each signal is assumed to have equal power. The correlation between each signal is assumed to be perfectly coherent because they are transmitted from the same wave source.

(2) Ray-Tracing Model

In the ray-tracing model, propagation paths from the wave source to measurement points are computed by the ray-tracing simulator, and DoAs are measured at each measurement point according to the path. In the ray-tracing simulator, we use the Furumachi area in the Niigata city. In

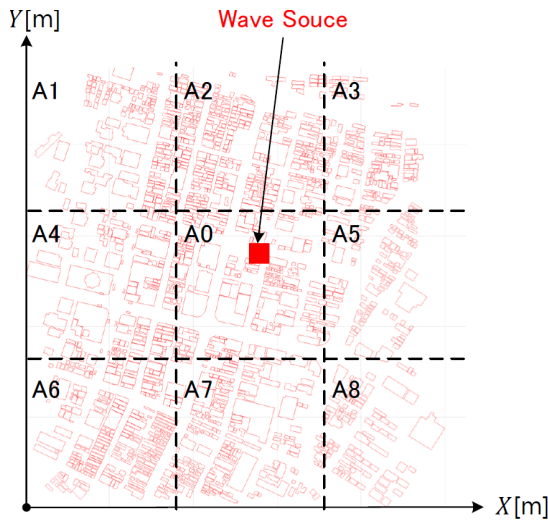


Fig. 12 Simulation area.

Table 3 Details pertaining to each area.

Area Number	M	h_i [m]	η_i [%]
Area 0	232	15.3	75
Area 1	142	12.1	94.5
Area 2	327	12.7	87.1
Area 3	151	15.6	84.3
Area 4	145	14.9	94.8
Area 5	119	17.7	63.9
Area 6	258	14.5	100
Area 7	208	14.0	100
Area 8	97	17.6	99

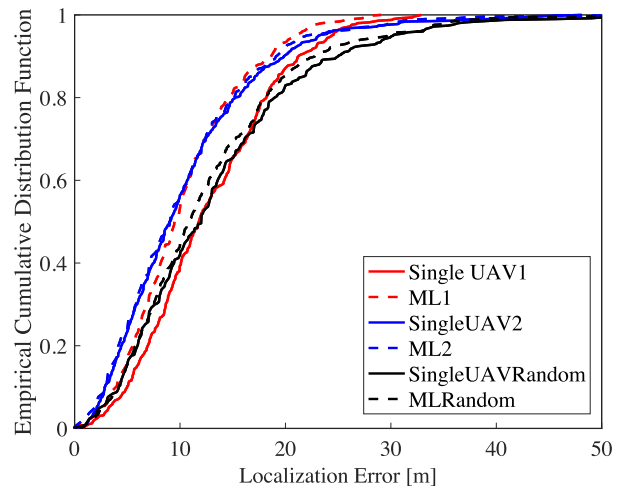
both the probabilistic and the ray-tracing models, the area has a size of 900×900 [m²] and is divided into 9 sub-areas A_0, A_1, \dots, A_8 with the same size of 300×300 [m²], as illustrated in Fig. 12. Table 3 lists the environment of the Furumachi area. Specifically, M_i, h_i, η_i ($i = 0, 1, \dots, 8$) in the table denote the number of buildings, average height of buildings, and probability that arbitrary point in the area is an NLOS environment in area A_i , respectively. The wave source v_0 is set randomly within the sub-area A_0 . When using the moving path planning algorithm 1 or 2, the initial position \mathbf{r}_1 is set randomly within the area $\bigcup_{i=1}^8 A_i$. When measurement points are placed randomly, i.e., the moving path planning algorithms are not adopted and all measurement points are placed randomly within the area $\bigcup_{i=1}^8 A_i$.

In both the probabilistic and ray-tracing models, simulations are conducted 500 times for each scheme. Let $\hat{\mathbf{r}}_0^{(i)}$ ($1 \leq i \leq 500$) denote the wave source location obtained from the i -th simulation. We define the wave source estimation error $\epsilon^{(i)}$ as

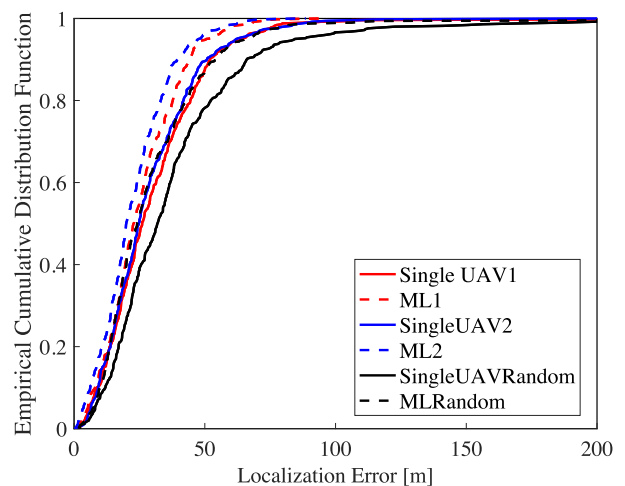
$$\epsilon^{(i)} = \|\hat{\mathbf{r}}_0^{(i)} - \mathbf{r}_0\|. \quad (5)$$

Root means square error $\bar{\epsilon}$ is defined as

$$\bar{\epsilon} = \sqrt{\frac{1}{500} \sum_{i=1}^{500} \epsilon^{(i)}}. \quad (6)$$



(a) Probabilistic Model



(b) Ray-Tracing Model

Fig. 13 Empirical cumulative distribution function of localization error $\epsilon^{(i)}$.

5.2 Simulation Results

Figure 13(a) illustrates the empirical cumulative distribution function (ECDF) of the localization error $\epsilon^{(i)}$ and the second column in Table 4 presents the mean localization error $\bar{\epsilon}$ in the probabilistic model. We observe that SingleUAV1 and SingleUAV2 exhibit lower mean estimation errors than SingleUAVRandom. Therefore, the moving path planning algorithms are effective in improving the localization error. ML1 and ML2 exhibit the better performance than SingleUAV1 and SingleUAV2. DoAs are generated according to the von-Mises distribution in the probabilistic model, and the likelihood function is formulated based on the same distribution. Therefore, ML1 and ML2 can obtain the optimal positions in terms of the maximum likelihood criterion.

Figure 13(b) illustrates the ECDF of the localization error $\epsilon^{(i)}$ and the third column in Table 4 presents the mean

Table 4 Mean localization errors $\bar{\epsilon}$.

	Probabilistic Model	Ray-Tracing Model
SingleUAV1	14.3 [m]	36.6 [m]
SingleUAV2	12.8 [m]	35.1 [m]
ML1	11.8 [m]	29.2 [m]
ML2	12.6 [m]	26.3 [m]
SingleUAVRandom	16.2 [m]	50.7 [m]
MLRandom	15.2 [m]	39.6 [m]

localization error $\bar{\epsilon}$ in the ray-tracing model. Similar to the probabilistic model, we observe that SingleUAV1 and Single UAV2 exhibit lower mean localization errors than SingleUAVRandom in the ray-tracing model. Comparing the wave source localization schemes in the probabilistic and ray-tracing models, mean localization errors $\bar{\epsilon}$ in the ray-tracing model are larger than those in the probabilistic model. We localize the wave source under the assumption that the mean value of DoAs coincides with the direction of the wave source. Furthermore, in the probabilistic model, DoAs are given such that the mean value coincides with the direction of the wave source. Therefore, in the probabilistic model, the wave source is localized with higher accuracy. Conversely, in the ray-tracing model, the DoA distribution highly relies on the structures around the wave source and measurement points. DoA does not necessarily coincide with the direction of the wave source. For example, if there is a large structure in a particular direction, then the DoAs from that direction cannot be obtained, and the mean of the DoAs deviates from the direction of the wave source. Figure 14 shows the empirical cumulative distribution function of the differences between the mean DoAs obtained for each UAV and the direction of the wave source for SingleUAV1 in the ray-tracing model. The figure shows that in most cases, the mean value of DoAs and direction of the wave source coincide. However, there are cases where the difference is more than 1 [rad]. This difference deteriorates the accuracy of wave source estimation.

In both the probabilistic and ray-tracing models, SingleUAV2 exhibits better performance than SingleUAV1. Therefore, although the moving path planning algorithm 2 cannot set an arbitrary number of measurement points, it can achieve finer localization than the moving path planning algorithm 1.

Note that both SingleUAV1 and SingleUAV2 cannot outperform ML1 and ML2, as demonstrated in the simulation results. However, the performance of the proposed scheme (i.e., SingleUAV1 and SingleUAV2) can be improved by extending it with the ML estimator. Figure 15 presents the extended scheme for the moving path planning algorithm 1. In the extended scheme, there are two estimators for the wave source v_0 . In the moving path planning algorithm 1, $r_0^{(n)}$ is sequentially estimated by the simplified estimator, as described in Sect. 4.4. After N measurement points are determined, the ML estimator estimates r_0 with $\{\mathcal{T}_n \mid n = 1, 2, \dots, N\}$. Evidently, the extended scheme has the same performance as ML1. Similarly, we can extend the moving path planning algorithm 2. In this case, the extended

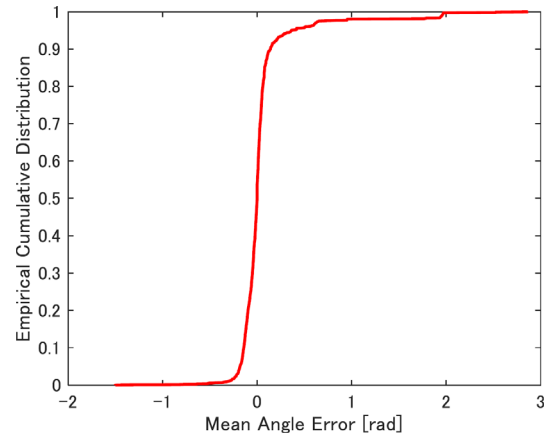


Fig. 14 Empirical cumulative distribution function of error in mean value of DoAs and direction of a wave source.

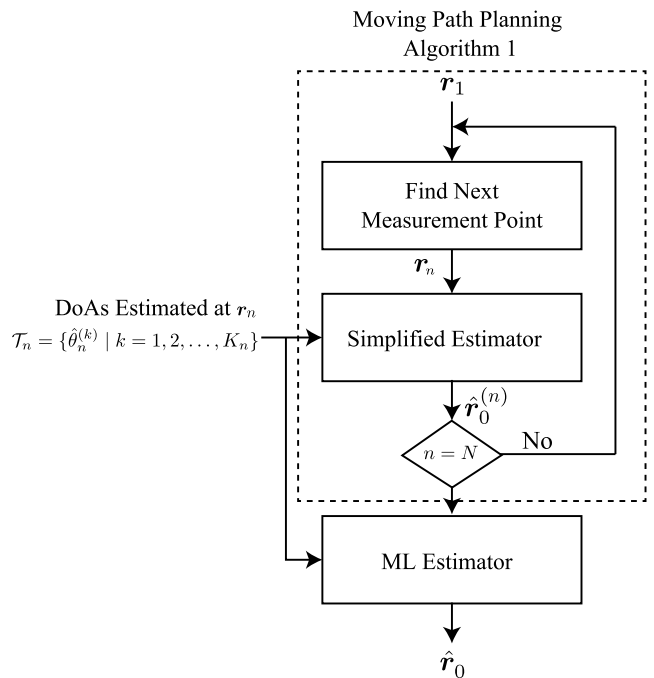


Fig. 15 Extension of the proposed scheme with the moving path planning algorithm 1.

scheme can achieve the same performance as ML2.

6. Conclusion

In this study, we proposed a single UAV-based wave source localization scheme that superimposes DoAs distributions estimated at measurement points of the UAV. To determine measurement points in the proposed scheme, we proposed two moving path planning algorithms. The performance of the proposed method was evaluated with the simulation experiments in the probabilistic and ray-tracing models. From the simulation results, it can be inferred that the proposed path planning algorithms are effective in actual urban environments that may contain outliers of DoAs. In this study,

the proposed method was evaluated under the assumption that only a single wave source exists in the target area. In the future, we will consider a method for multiple wave sources.

Acknowledgments

This work was supported in part by the MIC/SCOPE No. JP215004001, TMU local 5G research project, and TMU KAKENHI support.

References

- [1] N. Okello, "Emitter geolocation with multiple UAVs," Proc. 2006 9th International Conference on Information Fusion, July 2006.
- [2] F. Fletcher, B. Ristic, and D. Mušicki, "Recursive estimation of emitter location using TDOA measurements from two UAVs," Proc. 2007 10th International Conference on Information Fusion, July 2007.
- [3] D.J. Walter, K. Bryan, J. Stephens, C. Bullmaster, and V. Chakravarthy, "Localization of RF emitters using compressed sensing with multiple cooperative sensors," Proc. 2012 IEEE National Aerospace and Electronics Conference, pp.236–240, July 2012.
- [4] X. Fu, N.D. Sidiropoulos, J.H. Tranter, and W.K. Ma, "A factor analysis framework for power spectra separation and multiple emitter localization," IEEE Trans. Signal Process., vol.63, no.24, pp.6581–6594, Dec. 2015.
- [5] S. Takase, K. Nishimori, R. Taniguchi, T. Matsuda, and T. Mitsui, "Source location estimation via compressed sensing using UAVs," Proc. 2020 International Symposium on Antennas and Propagation (ISAP 2020), pp.237–238, Jan. 2021.
- [6] S. Murata, T. Matsuda, K. Nishimori, and T. Mitsui, "Circular statistics-based maximum likelihood estimation for wave source localization," Proc. IEEE International Symposium on Antennas and Propagation and North American Radio Science Meeting (APS/URSI 2020), July 2020.
- [7] S. Murata, T. Matsuda, and K. Nishimori, "Maximum likelihood estimation for single wave source localization using multiple UAVs in NLOS environments," IEICE Trans. Commun. (Japanese Edition), vol.J105-B, no.3, pp.229–239, March 2022.
- [8] S. Haykin, "Cognitive radio: Brain-empowered wireless communications," IEEE J. Sel. Areas Commun., vol.23, no.2, pp.201–220, Feb. 2005.
- [9] J. Urama, R. Wiren, O. Galinina, J. Kauppi, K. Hiltunen, J. Erkkilä, F. Chernogorov, P. Eteläaho, M. Heikkilä, J. Torsner, S. Andeev, and M. Valkama, "UAV-aided interference assessment for private 5G NR deployments: Challenges and solutions," IEEE Commun. Mag., vol.58, no.8, pp.89–95, Aug. 2020.
- [10] DEURAS system, <https://www.tele.soumu.go.jp/e/adm/monitoring/moni/type/deurasys/index.htm>
- [11] A. Haniz, G.K. Tran, R. Iwata, K. Sakaguchi, J. Takada, D. Hayashi, I. Yamaguchi, and S. Aarata, "Propagation channel interpolation for fingerprint-based localization of illegal radios," IEICE Trans. Commun., vol.E98-B, no.12, pp.2508–2519, Dec. 2015.
- [12] H. Krim and M. Viberg, "Two decades of array signal processing research: The parametric approach," IEEE Signal Process. Mag., vol.13, no.4, pp.67–94, July 1996.
- [13] E.J. Candès and M.B. Wakin, "An introduction to compressive sampling," IEEE Signal Process. Mag., vol.25, no.2, pp.21–30, March 2008.
- [14] K. Hayashi, M. Nagahara, and T. Tanaka, "A user's guide to compressed sensing for communications systems," IEICE Trans. Commun., vol.E96-B, no.3, pp.685–712, March 2013.
- [15] K.T. Wong, Y.I. Wu, and M. Abdulla, "Landmobile radiowave multipaths' DOA-distribution: Assessing geometric models by the open literature's empirical datasets," IEEE Trans. Antennas Propag., vol.58, no.3, pp.946–958, March 2010.
- [16] D.D.N. Bevan, A.G. Flaksman, V.T. Ermolayev, and I.M. Averin, "Gaussian channel model for mobile multipath environment," EURASIP J. Adv. Signal Process., vol.2004, no.9, pp.1321–1329, Aug. 2004.
- [17] N.I. Fisher, Statistical Analysis of Circular Data, Cambridge University Press, 1993.
- [18] S. Murata, T. Matsuda, K. Nishimori, and Tsutomu Mitsui, "Performance evaluation of wave source localization method using UAVs based on the maximum likelihood estimation," Proc. 2020 International Symposium on Antennas and Propagation (ISAP 2020), Jan. 2021.
- [19] S. Fortunati, R. Grasso, F. Gini, M.S. Greco, and K. LePage, "Single-snapshot DOA estimation by using compressed sensing," EURASIP J. Adv. Signal Process., vol.2014, p.120, July 2014.
- [20] Q. Shen, W. Liu, W. Cui, and S. Wu, "Underdetermined DOA estimation under the compressive sensing framework: A review," IEEE Access, vol.4, pp.8865–8878, Nov. 2016.
- [21] A. Beck and M. Teboulle, "A fast iterative shrinkage-thresholding algorithm for linear inverse problems," SIAM J. Imaging Sci., vol.2, no.1, pp.183–202, March 2009.



Shinichi Murata received his B.E. degree from the Kanagawa Institute of Technology, Japan, in 2013. He is currently a Ph.D. candidate in the Department of Computer Science, Graduate School of Systems Design, Tokyo Metropolitan University. His research interests include radio propagation and array antenna signal processing. He received the Best Paper Award from IEICE in 2023.



Takahiro Matsuda received his B.E. with honors, M.E., and Ph.D. degrees in communications engineering from Osaka University in 1996, 1997, 1999, respectively. He joined the Department of Communications Engineering at the Graduate School of Engineering, Osaka University in 1999. In the same department, he was an Assistant Professor from 1999 to 2005, a Lecturer from 2005 to 2009, and an Associate Professor from 2009 to 2018. He is currently a Professor in the Department of Computer Science, Graduate School of Systems Design, Tokyo Metropolitan University. His research interests include performance analysis and the design of communication networks and wireless communications. He received the Best Tutorial Paper Award and the Best Magazine Paper Award from IEICE ComSoc in 2012, and the Best Paper Award from IEICE in 2014 and 2023. He is a member of IPSJ and IEEE.